Experimental Study of Concrete Slab–Base Interaction for a Seamless Bridge–CRCP System

Xiaoyi Chen[1]; Behdad Mofarraj Kouchaki, Ph.D., A.M.ASCE[2]; Jay Malviya[3]; Juan Murcia-Delso[4]; Todd Helwig, M.ASCE[5]; and Jorge G. Zornberg, F.ASCE[6]

Abstract: Conventional bridge systems make use of expansion joints to accommodate movements caused primarily by thermal changes. These joints may accelerate the deterioration of bridge elements and often require significant maintenance costs. Originally proposed in Australia, the seamless bridge concept eliminates the need for expansion joints between bridge decks and roadway pavements. Past applications of seamless bridges have utilized a continuously reinforced concrete pavement (CRCP) in which a transition zone is employed between the bridge deck and the CRCP to accommodate the longitudinal expansion and contraction of the bridge and pavement. A critical aspect of the system response is the longitudinal load transfer mechanism in the transition zone, which is governed by the restraint at the concrete pavement–base interface. This paper presents an experimental investigation of the concrete slab–base interaction through unit-cell direct shear tests and cyclic full-scale push-off tests. The load (shear) versus displacement behavior at the interface was evaluated for different interface materials (geotextiles, polyethylene sheets, and felt paper). Test results indicated double-sided textured linear low-density polyethylene sheets and felt paper, which presented coefficients of friction of around 0.4 and 0.7, respectively, were the most promising interface materials to be considered for the transition zone. **DOI: 10.1061/JBENF2.BEENG-6076**.

Practical Applications: Seamless bridges provide a structural system that eliminates joints that permit corrosion-causing agents that adversely impact the super and substructure components. In seamless bridge systems, the bridge deck connects directly to a transition slab that provides a link with conventional pavement systems. The transition slabs deform to dissipate the thermal movements of the bridge. A critical element in the system is a bond breaker that allows the transition slabs to slide relative to the base foundation element. Too large of a coefficient of friction results in excessively wide cracks in the transition slabs, while too low of a friction coefficient results in excessive lengths of the transition slab region. This paper documents experimental studies on the performance of bond breakers to meet the needs of seamless bridge systems. The research considers the behavior of a wide variety of bond breakers with common bases used in bridge applications and recommends the most promising materials. These recommendations are critical to the successful implementation of seamless bridge systems in practice. The paper presents the results of a two-phase experimental program to identify the best bond breakers for seamless bridge systems and quantifies their interface resistance (coefficients of friction).

Introduction

Conventional bridge systems make use of expansion joints to accommodate movements caused primarily by thermal changes. Expansion joints are commonly located at the end of the bridge over the abutment or between adjacent spans over the intermediate piers for multispan bridges with precast concrete girders, as shown in Fig. 1(a). These expansion joints also provide a conduit for water, debris, and contaminants, which tend to accelerate the deterioration of the girders, bearings, and substructure elements. Accumulation of debris also frequently leads to locking of the joints, which can result in further deterioration of the deck or girders. In addition, expansion joints result in poor vehicular performance due to concentrated "bumps" at the ends of the bridge. These problems have spurred a number of studies that focused on the development of jointless bridges to decrease costs by simplifying periodic inspections as well as reducing the substantial maintenance demands that arise throughout the service life of the structure (Thippeswamy et al. 2002).

More recently, different types of jointless bridge technologies have been implemented to decrease the number of expansion joints, such as jointless deck bridges with the use of link slabs (Caner and Zia 1998; Wing and Kowalsky 2005; Au et al. 2013) [Fig. 1(b)], integral bridges (Civjan et al. 2007) [Fig. 1(c)], and semi-integral abutment bridges (White 2007; Burke 2009) [Fig. 1(d)]. While these concepts reduce the number of expansion joints or move

[1]Postdoctoral Fellow, Dept. of Civil, Architectural and Environmental Engineering, Univ. of Texas at Austin, 10100 Burnet Rd., Austin, TX 78758 (corresponding author). ORCID: https://orcid.org/0000-0002-4939-224X. Email: xiaoyi.chen@utexas.edu

[2]Dept. of Civil, Architectural and Environmental Engineering, Univ. of Texas at Austin, 301E. Dean Keeton St. ECJ 4.200, Austin, TX 78712-1700.

[3]Structural Designer, Holmes US, 235 Montgomery St., STE 1250, San Francisco, CA 94104.

[4]Assistant Professor, Dept. of Civil and Environmental Engineering, Polytechnic Univ. of Catalonia, C. Jordi Girona 1-3, 08034 Barcelona, Spain. ORCID: https://orcid.org/0000-0001-6424-7262.

[5]Jewel McAlister Smith Professor, Dept. of Civil, Architectural, and Environmental Engineering, Univ. of Texas at Austin, 10100 Burnet Rd., Austin, TX 78758.

[6]Brunswick-Abernathy Regents Professor, Dept. of Civil, Architectural and Environmental Engineering, Univ. of Texas at Austin, University Station, C1792, Austin, TX 78712-0280. ORCID: https://orcid.org/0000-0002-6307-1047.

Note. This manuscript was submitted on September 23, 2022; approved on February 1, 2023; published online on March 29, 2023. Discussion period open until August 29, 2023; separate discussions must be submitted for individual papers. This paper is part of the ***Journal of Bridge Engineering***, © ASCE, ISSN 1084-0702.

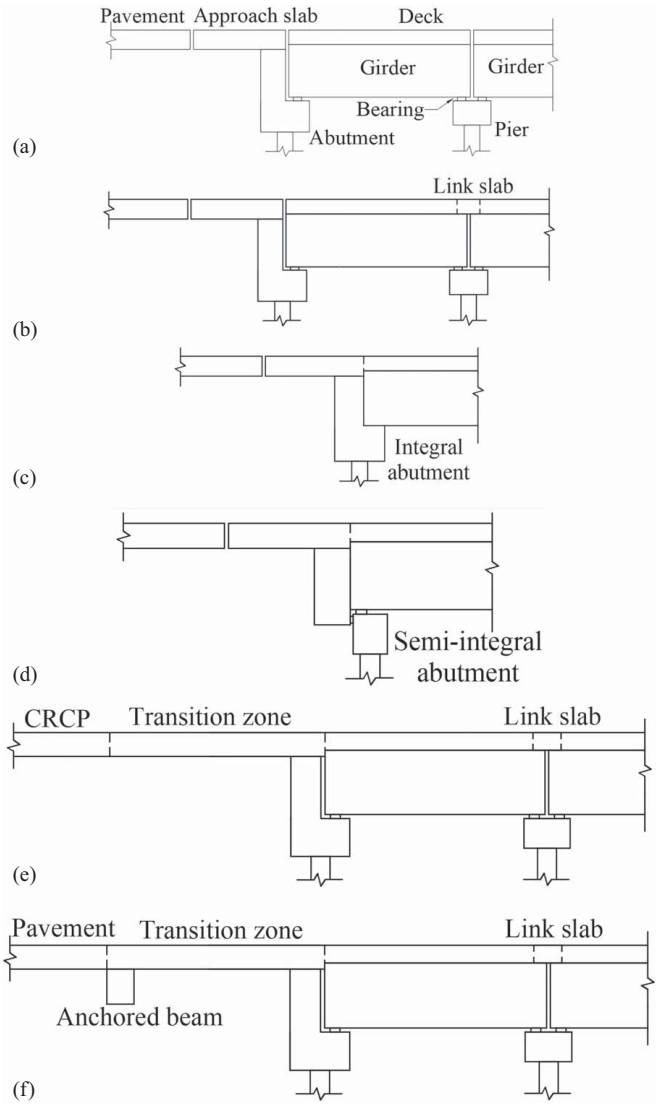

Fig. 1. Bridge types: (a) conventional jointed bridge–pavement system; (b) jointless deck bridge; (c) integral bridge; (d) semi-integral bridge; (e) seamless bridge–CRCP system; and (f) seamless bridge–pavement system with an anchor.

them to less critical locations, expansion joints are still required in the bridge–pavement system, which could be troublesome and expensive.

The seamless bridge concept originally implemented by Griffiths et al. (2005) in the Westlink M7 highway in Australia eliminates expansion joints at the end of the approach slab to make the bridge–pavement system fully jointless. This system features a transition zone that is seamlessly connected with continuously reinforced concrete pavement (CRCP), which is an excellent long-life performance solution for highly trafficked and heavily loaded roadways (Roesler et al. 2016), as shown in Fig. 1(e). Ala (2011) proposed a similar seamless bridge concept for flexible and jointed plain concrete pavements. In their system, the transition slab was connected via "small piles" to a "secondary slab" embedded in the base soil (Ala and Azizinamini 2016a, b). Another type of seamless bridge–pavement system reported in previous investigations involves an anchored beam at the end of the transition zone (Zhan et al. 2021), as shown in Fig. 1(f). The seamless connection can be considered analogous to a bridge–pavement "link slab." However, this structural form requires an anchored beam, and large axial forces may develop in the anchored beam end.

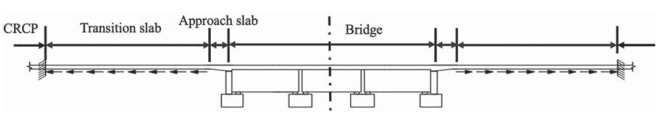

Fig. 2. Schematic of a seamless bridge–CRCP system.

Fig. 2 shows a schematic of a seamless bridge–CRCP system (showing a bridge undergoing contraction in this example). In a seamless system, the continuously connected transition zone between the bridge deck and the pavement accommodates time-dependent deformations. A bond breaker is placed between the base and the approach/transition pavements such that the pavement is able to slide on the base to accommodate the bridge movements. Due to the restraint provided by the jointless system, the transition zone is subjected to compressive forces during bridge expansion and tensile forces during bridge contraction. Fig. 3 shows an example to qualitatively illustrate the longitudinal movement and axial force expected in the transition slab. The figure indicates that beyond a certain distance from the bridge, the pavement is expected to no longer be affected by interactions with the bridge.

A critical aspect of the response of seamless bridge–pavement systems and the magnitude of tensile/compressive forces in the transition zone is the interaction between the pavement and the base layer and, more specifically, the coefficient of friction between the base and the pavement during sliding leading to frictional forces. The primary mechanism by which bridge deformations are accommodated during bridge contraction corresponds to distributed cracking within the reinforced concrete transition pavement. A major aspect for a successful implementation of seamless bridges is the need for proper characterization of the slab–base interaction for interface conditions typically used in the United States.

Push-off tests have been used to determine concrete slab–base interactions (Otto Rasmussen and Rozycki 2001). Lee (2000) has provided a good summary of past investigations on the characterization of concrete slab–base interactions. Past studies (Chia et al. 1986; Chan Suh et al. 2002; Maitra et al. 2009; Li et al. 2013; Jeong et al. 2014) have evaluated the effectiveness of several friction-reducing materials through push-off tests, including single and double layers of polyethylene (PE) sheets, curing compound, slurry seal, sand, thin asphalt layer, geotextile, and emulsified asphalt. For the seamless bridge project in Australia, field push-off tests were conducted to investigate different interface conditions (with two wax coats, bitumen seal, plastic sheets, and without debonding material) (Griffiths et al. 2005).

While previous work on slab–base characterization is insightful, an experimental evaluation of commonly used bases and interface materials remains, at best, incomplete. Another aspect requiring evaluation is the quantification of the expected movement in the concrete pavement of a seamless bridge system that must

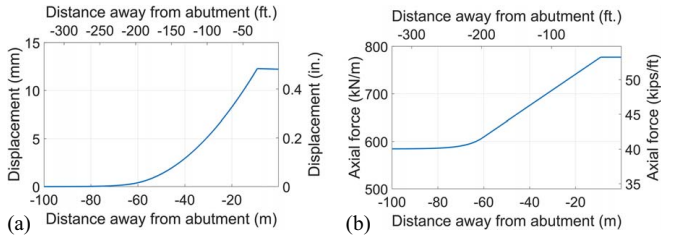

Fig. 3. Axial behavior of a transition slab: (a) longitudinal movement; and (b) axial force.

accommodate the induced deformations from bridge expansion/contraction in addition to the expansion/contraction of the pavement itself. A preliminary finite-element analysis of the axial behavior of a seamless CRCP-bridge system estimated pavement displacements up to 12.5 mm (0.5 in.) for a typical 90-m-long (295 ft long) bridge considering a maximum temperature decrease of 13°C (55°F) (TxDOT 2014; AASHTO 2020; Ha et al. 2012). However, previous experimental studies on the slab–base interaction have seldom considered such large displacements. Moreover, most of the experimental results reported in the literature were conducted in the case of a single level of normal load representing the weight of a typical pavement thickness. However, in seamless bridge applications, the thickness of the transition and approach slabs are often different and likely to vary for different bridge geometries. While the interaction force when bond breakers are present is expected to increase linearly with the normal force, and is characterized by a friction coefficient, experimental tests are needed for increasing normal forces to confirm the suitability of adopting a constant coefficient of friction. Finally, experimental data are needed to explore the potential use of alternate types of interface materials, such as spike/textured PE sheets and felt paper, as bond breakers in the transition zone of a seamless bridge system.

This paper outlines the results from an experimental investigation on the interaction between concrete slabs and common base materials, as well as on the effectiveness of different interface materials to act as bond breakers in the transition zone. These types of data are deemed essential for the analysis and design of seamless bridge systems. While primarily intended for CRCP, the results of this study could also be useful in applications of the seamless concept for other roadway pavements (e.g., flexible and jointed plain concrete pavements) in which CRCP is used only in the transition slab to dissipate bridge movements and eliminate the need for bridge expansion joints. The present study evaluates various interface materials as bond breakers, including different types of geotextiles and PE sheets as well as felt paper. The experimental program included two phases of testing involving different scales and types of loading. In Phase I, unit-cell direct shear tests were conducted to quantify the shear strength properties of relevant interfaces when subjected to monotonically increasing displacements. The Phase I studies allowed an identification of the best candidate materials for effective bond breakers to be subsequently considered in the Phase II studies. In Phase II, full-scale push-off tests were conducted on a select number of interfaces to verify the shear response considering a more representative scale and to quantify the effects of the cyclic loading. Both testing phases provided shear stress versus displacement relations for different normal stress levels and displacement levels up to 25 mm (1 in.). The experimentally obtained data were used to characterize the shear strength of the interfaces using a Mohr–Coulomb failure criterion. The results and findings of this study are discussed in relation to the potential use of bond breakers in the transition zone of a seamless bridge–CRCP system.

Behavioral Models for Concrete–Base Interaction

Following a classic Coulomb-friction model, the frictional characteristics of interfaces can be described using the coefficient of friction, μ, which is defined as follows:

$$\mu = \frac{F_{f0}}{N} = \frac{\tau_{f0}}{\sigma} \tag{1}$$

where τ_{f0} ($\tau_{f0} = F_{f0}/A$) and σ ($\sigma = N/A$) = frictional shear strength and normal stress at the interface, respectively; F_{f0} and N = frictional force and normal force at the interface, respectively; and A = area of the contact surface. The coefficient of friction, μ, which is determined by the nature of the materials and surface roughness, is appropriate for the characterization of the concrete slab–base if the physical nature is purely frictional. However, the concrete slab–base interaction may involve mechanisms associated not only to pure friction but also to interlocking and adhesion (Otto Rasmussen and Rozycki 2001). Considering the multiple interaction components, it is generally deemed appropriate to represent the interface shear strength using a Mohr–Coulomb failure criterion, which involves representing interface failure with a linear envelope relating normal and shear stresses. Accordingly, the shear strength of an interface can be represented by

$$\tau_f = a + \mu\sigma = a + \sigma \tan\delta \tag{2}$$

where τ_f = total shear strength at the interface; a = adhesion and/or interlock of material (or interface); and δ = interface friction angle. The parameters μ and a are generally defined as the slope and intercept of the linear regression line, respectively.

Another parameter, the apparent coefficient of friction, μ_{app}, is also defined:

$$\mu_{app} = \frac{F}{N} = \frac{\tau_f}{\sigma} \tag{3}$$

where F = total shear force at the interface ($F = \tau_f A$). In the case of pure friction, μ_{app} equals μ. In cases involving other interface resistance components, characterization using Mohr–Coulomb parameters μ and a allows a prediction of the interface shear strength for any normal stress, whereas characterization using μ_{app} only allows shear strength prediction for a specific normal stress.

Table 1 summarizes the frictional characteristics of concrete–base interfaces with different types of bond breakers reported from previous studies. The apparent coefficients of friction, μ_{app}, reported in Table 1, were defined using Eq. (3). Mohr–Coulomb parameters (μ and a) could be defined only when test results were reported for two or more normal stress levels. As shown in Table 1, experimental results in most previous studies were obtained at a single normal stress level, providing data that allow a determination of only the apparent coefficient of friction. This parameter only quantifies the interaction for a given slab thickness and cannot be directly extrapolated to other thicknesses. Among the different materials previously investigated, PE sheets (single or double layer) were generally shown to be effective bond breakers, with μ_{app}values ranging between 0.5 and 0.9. As a reference, μ_{app} value used for the design of CRCP without bond breakers ranged from 3.5 to 13 (Roesler et al. 2016).

Phase I: Unit-Cell Direct Shear Tests

The base materials investigated were primarily a cement-stabilized base (CSB) and a hot mix asphalt (HMA) base, which are durable, stabilized, and nonerodible bases typically constructed under CRCP. Granular base materials, such as AASHTO Gravel no. 8 and TxDOT Grade 3 Aggregate (TxDOT 2014), were also considered. AASHTO Gravel no. 8 is a moisture-insensitive material and therefore helpful for density control, which is a desired feature for the baseline test. Grade 3 Aggregate was selected because it can be used as backfill material underneath the concrete approach slab, which is a part of the transition zone in a seamless bridge–pavement system. The bases used in Phase I are shown in Fig. 4.

The following interface materials (Fig. 5) were considered in the Phase I testing program:

- PE sheets (ASTM E1745-17, ASTM 2017b). These sheets present a wide range of densities and surface structures (e.g.,

Table 1. Concrete slab–base interaction with bond breakers from previous studies

Base type	Interface material	Test data			Mohr–Coulomb parameters		Reference
		σ (kPa/psi)	τ (kPa/psi)	μ_{app}	μ	a (kPa/psi)	
Sand	PE sheet	3.2/0.47	1.8/0.26	0.56	Insufficient information		Stott (1961)
Medium-textured| CSB	1.6 mm (1/16in.) sand skin + PE sheet	3.4/0.5	2.5/0.36	0.74	0.69	0.14/0.02	Wimsatt et al. (1987)
		7.0/1.01	4.7/0.68	0.67			
		7.0/1.01	5.0/0.73	0.71			
	Double PE sheets	3.4/0.5	2.5/0.36	0.74	Insufficient information		
	1.6 mm (1/16 in.) sand skin		4.3/0.63	1.26			
Sand-mix asphalt base	Single PE sheet	3.4/0.5	3.0/0.44	0.88	Insufficient information		Chia et al. (1986)
	Double PE sheets		1.7/0.24	0.5			
	Spray compound with oil		11.1/1.61	3.26			
Lean concrete	Single PE sheet	4.5/0.66	2.6/0.38	0.58	0.57	0.14/0.02	Chan Suh et al. (2002)
		9.0/1.32	5.4/0.78	0.60			
		13.5/1.98	7.8/1.13	0.58			
	Asphalt layer (40-mm-/1.57-in.-thick)	4.5/0.66	4.6/0.67	1.02	0.6	1.80/0.26	
		9.0/1.32	6.9/1.00	0.77			
		13.5/1.98	10.1/1.47	0.75			
Cement-stabilized crushed stone	Single PE sheet	5.9/0.86	3.7/0.54	0.63	Insufficient information		Li et al. (2013)
	Geotextile		4.7/2.13	2.49			
	Emulsified asphalt		45.2/6.55	7.66			
	Asphalt layer (19-mm-/0.75-in.-thick)		11.0/1.60	1.86			

smooth, spiked, textured). PE sheets are geosynthetics widely used for containment purposes and can also be used as bond breakers. For example, in South Korea, PE sheets have been widely used as bond breakers between lean concrete bases and concrete pavements (Jeong et al. 2014). Specifically, 0.15-mm-thick (6-mil-thick) PE sheets were selected.

- Woven or nonwoven geotextiles. These geosynthetics are commonly used for separation, filtration, or reinforcement purposes. In Germany, nonwoven geotextiles have been adopted successfully as bond breakers between a cementitious base and a newly paved concrete for years (Cackler et al. 2018).
- Thin HMA layer (usually 25-mm-/1-in.-thick). An HMA layer has been commonly used for stress-relieving purposes between CSB and concrete pavements (TxDOT 2019). An HMA layer can be utilized in addition to a bond breaker at the interface between transition slabs and bases.

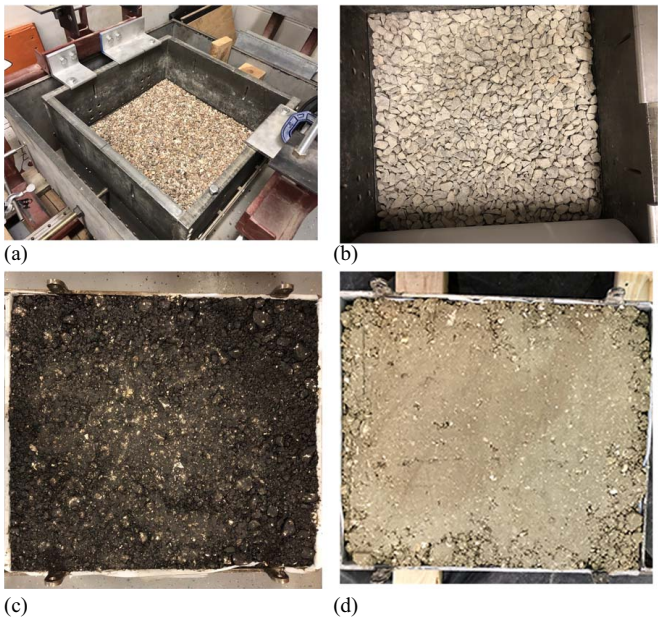

Fig. 4. Phase I bases: (a) AASHTO Gravel no. 8; (b) TxDOT Grade 3 Aggregate; (c) HMA; and (d) CSB.

Test Setup and Instrumentation

A unit-cell direct shear test setup previously used to characterize the shear strength of aggregate materials (Mohamed 2017) was employed in this study to characterize the concrete slab–base interaction with different interface conditions, as shown in Fig. 6. The test

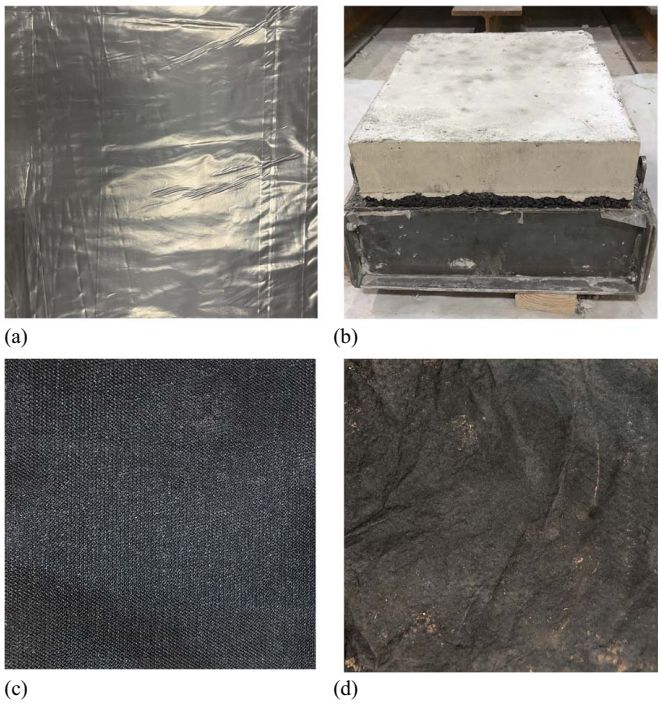

Fig. 5. Phase I interface materials: (a) PE sheet; (b) thin HMA; (c) woven geotextile; and (d) nonwoven geotextile.

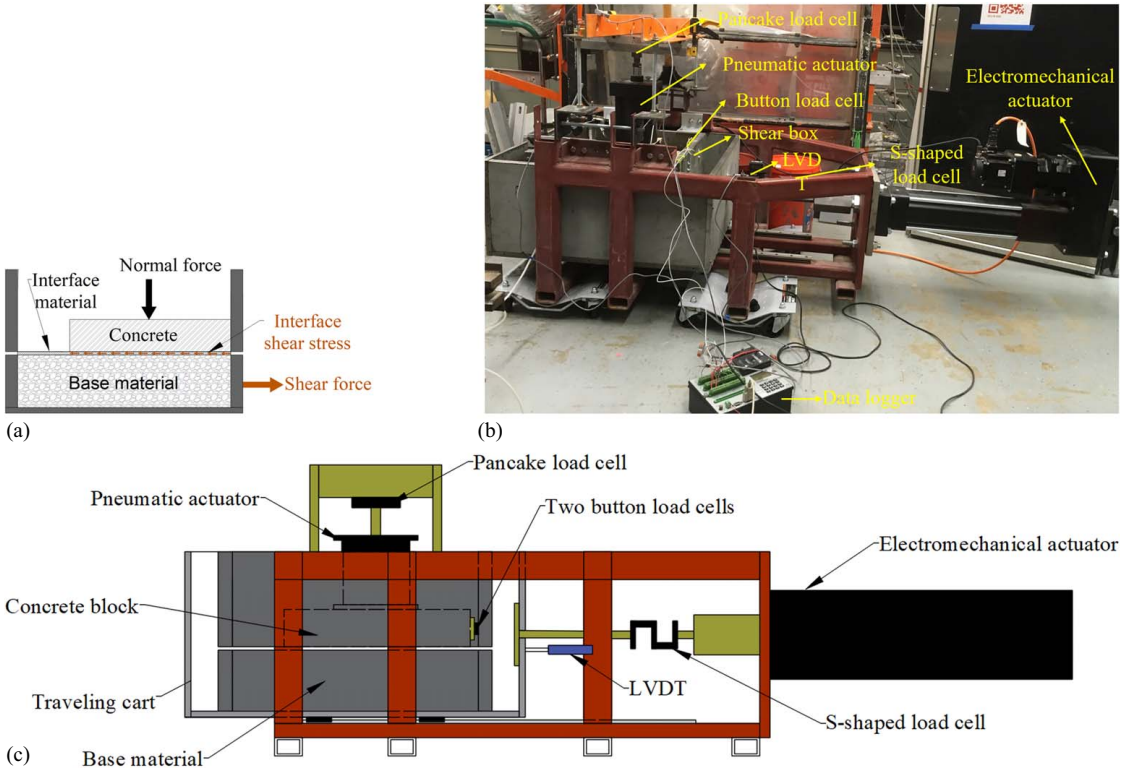

Fig. 6. Phase I unit-cell direct shear test setup and instrumentation: (a) schematic of a specimen box; (b) photo of the entire setup; and (c) schematic of the entire setup.

setup, depicted in Fig. 6(a), includes a specimen container (box), with inner plane dimensions of 0.5 m × 0.5 m (20 in. × 20 in.), divided into two halves that can move independently, which facilitates testing of the concrete–base interface under shear. Figs. 6(b and c) show the photo and schematic of the entire setup, respectively. This self-reacting system involves a horizontal reaction frame that applies shear forces at the interface via an electromechanical actuator and a vertical reaction frame that applies normal forces on top of the concrete via a pneumatic actuator. During testing, the base in the lower portion of the direct shear box was pulled/pushed in relation to the concrete block contained in the upper portion of the box, which reacted laterally against the test frame.

Fig. 6(c) presents the instrumentation used in the test setup. A linear variable differential transformer (LVDT) with a range of 76 mm (3 in.) was attached to the side of the traveling cart to measure the horizontal displacement of the base relative to the concrete block. A pancake load cell with a capacity of 22.2 kN (5 kips) was used to measure the normal force applied on top of the concrete block. Since the magnitude of the interface shear strength was expected to vary significantly depending on the interface conditions, two sets of horizontal load cells with different capacities were employed for different test series. One set included an S-shaped load cell with a capacity of 44.5 kN (10 kips) installed between the electromechanical actuator and the traveling cart to measure the horizontal force component introduced by the actuator. The load cell reading also included the frictional forces generated between the rail guides and the traveling cart, because the setup was not completely frictionless; however, the error introduced by this component was negligible in cases in which adhesion generated larger interface shear forces. Consequently, the S-shaped load cell was used for the test series when a large shear force was expected with a strong bond at the interface. Two button load cells with a capacity of 8.9 kN (2 kips) were placed against the top half of the shear box, the readings from which eliminated rail friction and provided direct measurement of the interaction at the interface. These smaller-capacity load cells were added to improve the accuracy of the test series in which a small shear force was expected with the use of a bond breaker.

Test Parameters and Procedure

Eleven test series involving different combinations of bases and interface materials were conducted, as presented in Table 2. Direct shear tests were conducted in cases of three predetermined normal stresses of 3.5 kPa (0.5 psi), 8 kPa (1.17 psi), and 13.8 kPa (2 psi), representing the weight of concrete pavement with thicknesses of 0.15 m (6 in.), 0.35 m (14 in.), and 0.6 m (24 in.), respectively. The first two thicknesses correspond to the range of conventional CRCP, while the third was selected to generate a higher level of normal stress for a better characterization of the shear strength failure envelope. The thickness of the concrete blocks employed in the tests was 0.08 m (3 in.), with dead weights being added by a vertical actuator to achieve the target normal stress at the interface.

For simplicity in testing, precast concrete specimens were considered to be used on various interface conditions (Series 1–3). The effects of using a precast concrete block (no bond with the base/interface material) on the interface restraint were also investigated by comparing the results of Series 3a and 3b. For most of the test series, cast-in-place (CIP) concrete was used on top of the base or interface material to be as representative of field conditions as possible. Tests were conducted with monotonically increasing displacements at a rate of 0.6 mm/min (0.0236 in./min) until a 25 mm (1 in.) displacement was reached or an obvious steady shear resistance was observed.

The guidelines for base construction in the State of Texas (TxDOT 2014) were followed for the preparation of the HMA

Table 2. Phase I test matrix

Series	Base type	Interface material	Concrete block	Normal stress	
				kPa	psi
1	AASHTO Gravel no.8	None	Precast	3.5, 8, 13.8	0.5, 1.17, 2
2	Grade 3 Aggregate	None	Precast	3.5, 8, 13.8	0.5, 1.17, 2
3a	Grade 3 Aggregate	Two PE sheets	Precast	3.5, 8, 13.8	0.5, 1.17, 2
3b	Grade 3 Aggregate	Two PE sheets	CIP	8	1.17
4	Type B HMA base	None	CIP	8	1.17
5	Type B HMA base	Two PE sheets	CIP	3.5, 8, 13.8	0.5, 1.17, 2
6	CSB	None	CIP	8	1.17
7	CSB	Thin type D HMA	CIP	8	1.17
8	CSB	Woven geotextile	CIP	8	1.17
9	CSB	Nonwoven geotextile	CIP	8	1.17
10	CSB	One PE sheet	CIP	3.5, 8, 13.8	0.5, 1.17, 2
11	CSB	Two PE sheets	CIP	3.5, 8, 13.8	0.5, 1.17, 2

and CSB specimens in the laboratory. Table 3 lists the aggregate gradations for the Type B and Type D HMA, which are typically used for the base and interface layer, respectively. In Table 4, the mix characteristics for the Type B and Type D HMA can be found.

The cement content by weight of CSB was 5%. CSB cylindrical specimens were prepared for unconfined compressive strength testing in accordance with ASTM D588-19 (ASTM 2019). The CSB compressive strength obtained at 7 days after placement, based on ASTM D1633-17 (ASTM 2017a), was 6.34 MPa (900 psi), which satisfies the minimum specimen strength requirement of 3.45 MPa (500 psi) established in TxDOT (2014). The concrete mix design for the slabs is presented in Table 5. The mix had a water/cement ratio of 0.49, a specified slump of 127 mm (5 in.), and a measured slump ranged from 100 to 150 mm (4–6 in.). The concrete compressive strengths measured on the 28th day after casting, in accordance with ASTM C39-21 (ASTM 2021), ranged from 28 to 35 MPa (4,000–5,000 psi), which satisfies the minimum requirement of 27.6 MPa (4,000 psi) (TxDOT 2014).

Phase I: Experimental Results and Discussion

Shear Stress–Displacement Relations

The concrete slab–base interaction may vary significantly depending on the types of base and interface materials. The shear force and shear displacement for each test series were recorded during testing. Assuming a uniform distribution of shear stresses over the entire interface contact area, the shear stresses were correspondingly obtained as a result of dividing the total shear force by the contact area. Selected shear stress versus displacement relationships are shown in Fig. 7. In Fig. 7(a), the results for Grade 3 Aggregate base with two PE sheets (Series 3a and 3b) are presented. For the tests involving a precast concrete block, the shear resistance increased until the preliminary displacement was reached, followed by a plateau where steady sliding occurred. Similar trends were observed for Series 1 and 2 for granular bases with a precast concrete block. For the tests involving a CIP concrete, the peak shear stress was reached at approximately 10 mm (0.4 in.) displacement. After the peak, the shear stress gradually decreased until a plateau occurred at approximately 20 mm (0.8 in.) displacement. An evaluation of the results from Series 3a and 3b revealed that the coefficient of friction of the interface was 1.5 times higher for the tests involving a CIP concrete block than when using a precast concrete block. This was likely due to the matching texture of the concrete cast against the interface generating a rougher profile, whereas the precast concrete block tended to slide on the high points of the base. It was concluded that testing involving precast concrete test specimens is not representative of the overall interface behavior expected in the field, even in the presence of interface materials acting as bond breakers. This is because the specimens fail to capture the adhesive component with the interface material that adds to the mechanical interlock generated when concrete is directly cast. Therefore, in subsequent test series, concrete specimens were directly cast over the interface to better represent the expected field conditions.

Table 3. HMA mix aggregate gradations

HMA	Sieve size (mm/in.)	25–30/1–1.2	25/1	19/0.75	9.51/0.38	4.76/#4	2.38/#8	0.56/#30	0.3/#50	0.07/#200
Type B (base)	Percent passing (%)	100	99.2	93.2	74.5	49.7	35.0	22.4	16.1	5.0
Type D (interface)		100	100	100	93.9	61.0	39.4	23.8	16.6	4.5

Table 4. HMA mix characteristics

HMA	Asphalt content (%)	Theoretical maximum specific gravity	Void in mineral aggregates (%)
Type B (base)	4.5	2.569	13
Type D (interface)	5	2.549	15

Table 5. Concrete mix design

Material type	Weight (kg/m^3 or lbf/yd^3)
Cement	244/412
Fly ash	82/138
Coarse aggregate	1,008/1,700
Fine aggregate	801/1,351
Water	118/200

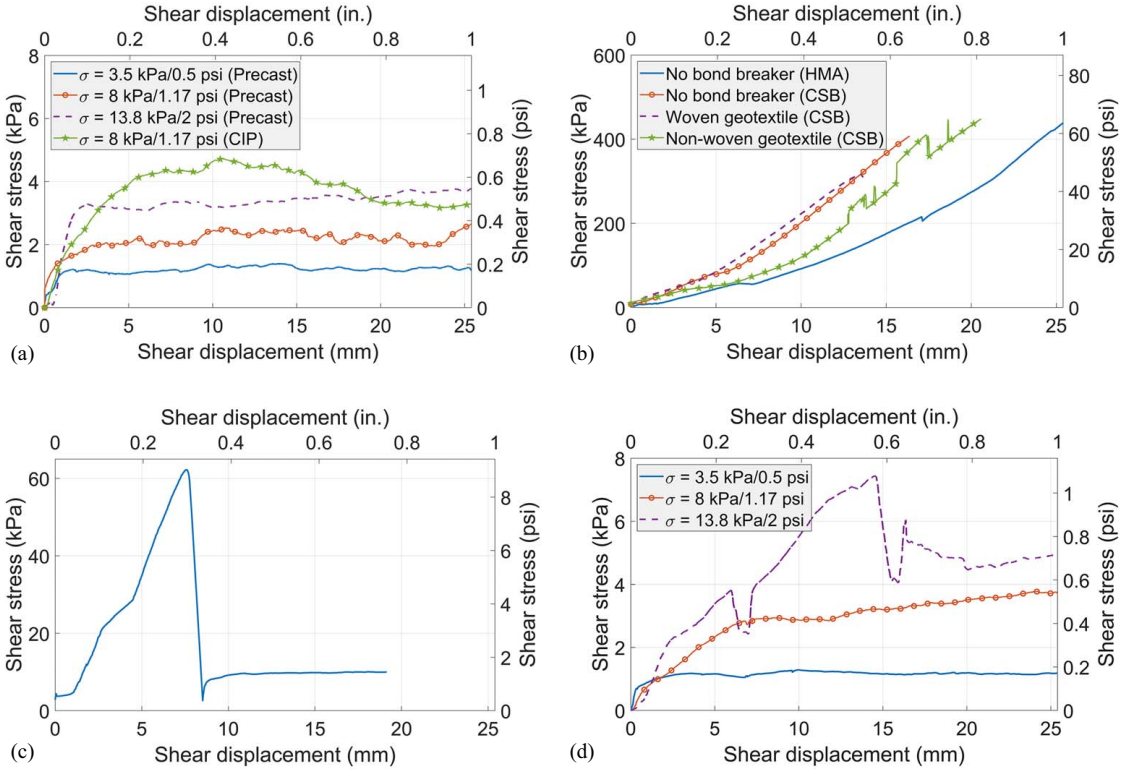

Fig. 7. Phase I shear stress–displacement relationships: (a) two PE sheets (Grade 3 Aggregate); (b) strong interfaces (CSB or HMA) (σ = 8 kPa/1.17 psi); (c) thin HMA layer (CSB) (σ = 8 kPa/1.17 psi); and (d) two PE sheets (HMA).

Fig. 7(b) shows the shear stress–displacement relationships for the interface test results that led to comparatively high shear stresses. All test results involved CIP concrete placed directly over the interface. In the test involving concrete placed on the HMA base or CSB (Series 4 and 6), the maximum force was limited by the capacity of the test setup, so ultimate failure at the slab–base interface was not reached before stopping the test. Such results reveal that a strong adhesion develops at the interface. Similarly, interface failure was not reached for the tests involving a nonwoven geotextile placed between the CSB and the concrete (Series 9). The CSB and woven geotextile specimen (Series 8) eventually failed at the interface, but at a relatively high shear stress of 315 kPa (45 psi). Sliding occurred at the interface between the CSB and the woven geotextile, whereas the concrete block remained attached to the geotextile. In this case, cement paste from the concrete was observed to have permeated the geotextile and bonded with the CSB during casting, which caused the comparatively high interface shear strength.

The use of a thin HMA layer (Series 7) resulted in a significant decrease in the interface strength, but still resulted in a peak strength of 62 kPa (9 psi), indicating the existence of adhesion at the CSB–HMA interface. As depicted in Fig. 7(c), at approximately 7.5 mm (0.3 in.) shear displacement, the bond was broken and the shear stress dropped significantly from its peak value to a plateau of approximately 10 kPa (1.4 psi). The concrete block was observed to slide along with the thin HMA layer relative to the CSB. The results from tests conducted in the case of a normal stress of 8 kPa (1.17 psi) indicated that the thin HMA layer and the woven and nonwoven geotextiles investigated in this study were not suitable to function as bond breakers for the concrete slab–base interface. This is because if used in the transition slab of a seamless bridge system, this type of interface would generate high axial forces and lead to severe cracking issues. Therefore, no further tests were conducted with these interface conditions for other normal stresses.

For the HMA/CSB with PE sheets (Series 5, 10, and 11), the shear stress–displacement relationships presented similar trends. As an example, Fig. 7(d) shows the results of tests conducted with HMA and two PE sheets. The same specimen was used in the subsequent tests at different normal stresses with a testing order consisting of 13.8 kPa (2 psi), 8 kPa (1.17 psi), and 3.5 kPa (0.5 psi). A well-defined peak strength was observed in the first test conducted in the case of 13.8 kPa (2 psi) normal stress. For the other two normal stresses, peak strength values had not been reached by the maximum displacement of the test setup of 25 mm (1 in.), probably because much of the interlocking that developed in the initial test (13.8 kPa/2 psi) may have been lost during the subsequent tests.

For the interfaces with the use of CIP concrete examined in this study, either with or without bond breakers, the shear stress–displacement curve exhibits a pattern involving a well-defined interface peak shear strength, followed by a drop, and finally a steady (or residual) strength, as shown in Fig. 8. For some strong interfaces that could not be failed (Series 4, 6, and 9), only an initial

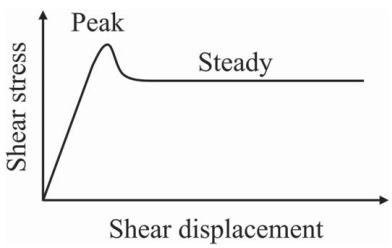

Fig. 8. Typical shape of shear stress–displacement relationship.

Table 6. Phase I results of concrete slab–base interaction

Series	Base type	Interface material	Concrete	Mohr–Coulomb parameters	
				μ	a (kPa/psi)
1	AASHTO no. 8	None	Precast	0.36	0.28/0.04
2	Grade 3 Aggregate	None	Precast	0.38	0.34/0.05
3a	Grade 3 Aggregate	Two PE sheets	Precast	0.19	0.62/0.09
3b	Grade 3 Aggregate	Two PE sheets	CIP	$\mu_{app\_peak\ (\sigma=8\,kPa/1.17\,psi)} = 0.57$ $\mu_{app\_steady\ (\sigma=8\,kPa/1.17\,psi)} = 0.40$	
4	Type B HMA	None	CIP	$\mu_{app\_peak\ (\sigma=8\,kPa/1.17\,psi)} > 54$	
5	Type B HMA	Two PE sheets	CIP	0.35	0
6	CSB	None	CIP	$\mu_{app\_peak\ (\sigma=8\,kPa/1.17\,psi)} > 50$	
7	CSB	Thin type D HMA	CIP	$\mu_{app\_peak\ (\sigma=8\,kPa/1.17\,psi)} = 7.7$ $\mu_{app\_steady\ (\sigma=8\,kPa/1.17\,psi)} = 1.2$	
8	CSB	Woven geotextile	CIP	$\mu_{app\_peak\ (\sigma=8\,kPa/1.17\,psi)} = 39$	
9	CSB	Nonwoven geotextile	CIP	$\mu_{app\_peak\ (\sigma=8\,kPa/1.17\,psi)} > 56$	
10	CSB	One PE sheet	CIP	0.2	0.21/0.03
11	CSB	Two PE sheets	CIP	0.15	0.14/0.02

portion of the stress–displacement curve was obtained. The peak can be attributed to two sources of interface resistance. One source is the interlocking effect of the matching profiles between the top surface of the base and the bottom surface of the CIP concrete block. This interlocking effect explains the small peaks observed with PE sheets. The interface shear strength dropped 35% (from 7.7 to 4.8 kPa/1.12 to 0.7 psi) after the interlocking mechanism was broken for the HMA with two PE sheets. The second source of the initial peak in the shear stress–displacement response is the adhesion of the interface, which may contribute significantly to the interface shear strength. For the CSB with a thin HMA layer, the shear strength dropped 85% (from 62 to 10 kPa/9 to 1.4 psi) following the peak, which indicates a notable initial adhesion component. Once the initial adhesion and/or interlocking mechanism is broken, the shear stress decreases and tends to exhibit a plateau.

Interface Shear Strengths and Friction Coefficients

Table 6 summarizes the results of the Phase I testing program in terms of the Mohr–Coulomb parameters defined for each interface condition. The shear strength at failure used in the strength envelope corresponds to the steady interface shear strength, which has also been identified in the literature as the large–displacement interface shear strength.

For the test series conducted at three normal stress levels (Series 1, 2, 3a, 5, 10, and 11), shear strength envelopes were obtained by plotting three sets of normal stresses and shear stresses at failure, and correspondingly, Mohr–Coulomb parameters, μ and a, were reported. For the remaining test series that presented a strong interaction, tests were conducted only for a normal stress of 8 kPa (1.17 psi), and the corresponding apparent coefficient of friction was reported. For the tests involving interfaces for which ultimate failure could not be achieved within the loading capacity of the testing device (i.e., Series 4, 6, and 9), only a lower bound of the apparent coefficient of friction, μ_{app}, was calculated using the measured maximum shear stress. The use of PE sheets significantly decreased the shear strength at the CIP concrete–CSB and CIP concrete–HMA interface by effectively eliminating the adhesion. This is evidenced by the small values of the a coefficient (intercept) of the resulting Mohr–Coulomb relation, as shown in Table 6. The coefficient of friction provided by two layers of PE sheets was slightly lower than that obtained using only one layer.

Phase II: Full-Scale Push-Off Tests

Based on an assessment of Phase I test results, the only bond breakers to fully eliminate the bond with the CIP concrete were the specimens with one or two PE sheets at the interface. Consequently, PE sheets were further examined in Phase II with full-scale slab segments. Furthermore, the following two types of PE sheets with surface roughness were added to the test program: (1) a 1-mm-thick (40-mil-thick) spike high-density polyethylene (HDPE) sheet with single-sided 0.5 mm (20 mil) asperities; and (2) a 1.5-mm-thick (60-mil-thick) double-sided textured linear low-density polyethylene (LLDPE) sheet. LLDPE sheets generally have higher tensile strength or resistance to harsh environments compared with the 0.15-mm-thick (6-mil-thick) PE sheets in Phase I testing. LLDPE sheets are also more flexible than HDPE sheets, which simplifies handling during construction. Another practical bond breaker that was added in Phase II consisted of asphalt-

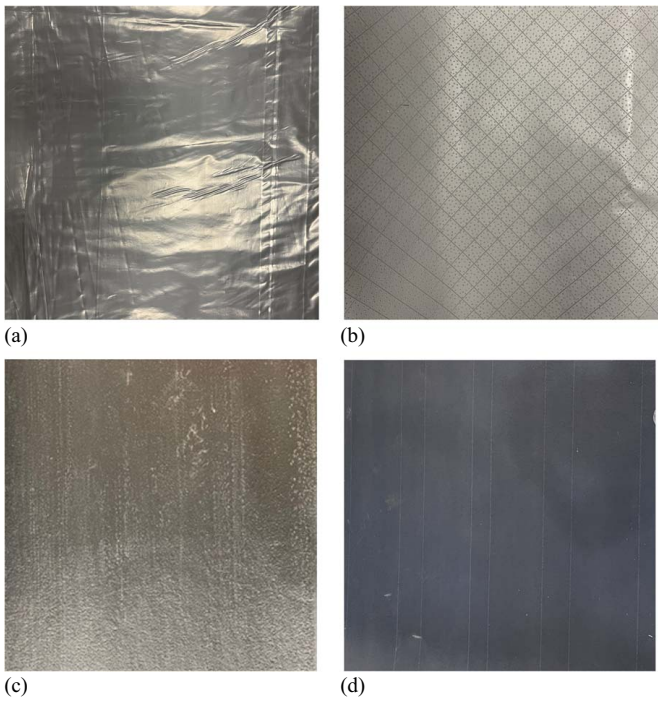

Fig. 9. Phase II interface materials: (a) PE sheet; (b) spike HDPE sheet; (c) textured LLDPE sheet; and (d) felt paper.

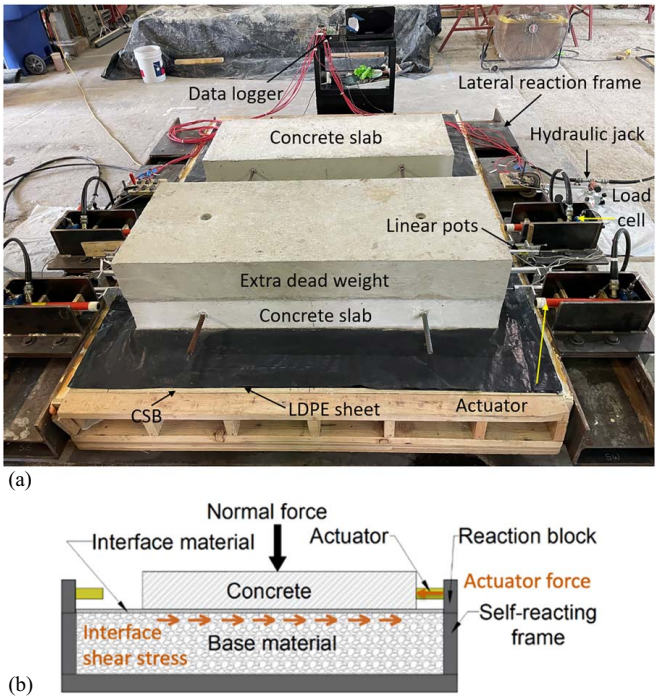

Fig. 10. Phase II full-scale push-off test setup and instrumentation: (a) photo; and (b) schematic.

saturated organic felt paper, which is impermeable and has previously been used in bridge applications as bearings for pan girders. The specific material tested was Type II felt paper (ASTM D4869-16, ASTM 2016). The interface materials used in Phase II are shown in Fig. 9.

Test Setup and Instrumentation

The Phase II experiments involved full-scale push-off tests on concrete slabs subjected to fully reversed cyclic displacement demands. To facilitate the testing program, two identical self-reacting test frames, one of which can be seen in Fig. 10(a), were designed and fabricated to conduct the push-off tests. Each frame could accommodate two test specimens. The mechanism for the full-scale tests, with various components labeled, is depicted in Fig. 10(b). The test setup consists of a support frame and lateral reaction frame. The test specimens include a compacted base with the dimensions of 2.4 m × 1.8 m × 0.18 m (8 ft × 6 ft × 7 in.) inside a wooden box, a CIP concrete slab with the dimensions of 1.5 m × 0.6 m × 0.15 m (5 ft × 2 ft × 6 in.), and an interface material between the base and the slab. The specimens were prepared on top of the support frame. The lateral reaction frame consists of two identical wide flange beams, one on each side of the wooden box, perpendicular to the loading direction. The lateral beams restrain the movement of the base and are bolted to the bottom beams to transfer the horizontal force.

Two single-acting hydraulic cylinders were used on each side to push the concrete slab in two opposite directions consecutively. When the cylinders on one side pushed the slab, the cylinders on the opposite side were fully retracted and not in contact with the slab. The use of two cylinders on each side led to a uniform sliding of the slab and mitigated the rotational effects around the vertical axis of the concrete slab during testing. The force applied by the hydraulic cylinders was measured via load cells with a capacity of 8.9 kN (2 kips), and the interface shear force was calculated by adding the two readings. A total of four linear potentiometers with a range of 102 mm (4 in.) were mounted on the lateral reaction frame (two on each side) to measure the displacement of the concrete slab relative to the base. The relative horizontal displacements were obtained by averaging the four readings.

Table 7. Phase II test matrix

Series	Base type	Bond breaker
1	CSB (#1 and #2)	Two PE sheets
2	CSB (#1 and #2)	One PE sheet
3	CSB (#1)	Single-sided spike HDPE sheet
4	CSB (#1)	Double-sided textured LLDPE sheet
5	CSB (#1)	Felt paper
6	CSB (#2) with thin Type D HMA	Double-sided textured LLDPE sheet
7a	CSB (#2) with thin Type D HMA	Felt paper
7b	CSB (#2) with thin Type B HMA	Felt paper

Test Parameters and Procedure

Table 7 summarizes the test matrix for Phase II, which focused on CSB with bond breakers. Two CSB specimens with identical mix designs were prepared in Phase II, as pictured in Fig. 11(a). Two different mixtures were used for the CSB, yielding a noticeable difference in the finished surface. Test series 1 and 2 were repeated on both CSB Specimens #1 and #2. Due to the observable difference in CSB finishes, the results provide an insight into the effects of the slight variances in the CSB finished surfaces on the coefficient of friction. Additionally, CSB topped with a 25-mm-thick (1-in.-thick) HMA layer was considered as a base type (Series 6 and 7). In some U.S. states (Roesler et al. 2016), a thin HMA layer is routinely constructed under the normal CRCP, so continuing a thin HMA layer to the transition slab might be a preferable construction procedure to accommodate the difference in thickness. Test series 6 and 7 provide the concrete slab–base interactions with different types of bond breakers for such conditions. Furthermore, Type B and Type D HMA are usually used for the HMA base and thin HMA interface layer, respectively. Test series 7a and 7b specifically investigate the effects of Type D and Type B HMA on interface characteristics. Fig. 11(b) presents the surface of Type B and Type D HMA layers on top of the CSB specimen.

For each interface condition, push-off tests were conducted in the case of three normal stresses, consistent with Phase I, of 3.5 kPa (0.5 psi), 8 kPa (1.17 psi), and 13.8 kPa (2 psi). The concrete slab specimen had a thickness of 0.15 m (6 in.) corresponding to the 3.5 kPa (0.5 psi) normal stress level. Two additional concrete slabs with identical plane dimensions, but different thicknesses of 0.2 m (8 in.) and 0.25 m (10 in.), were constructed for additional

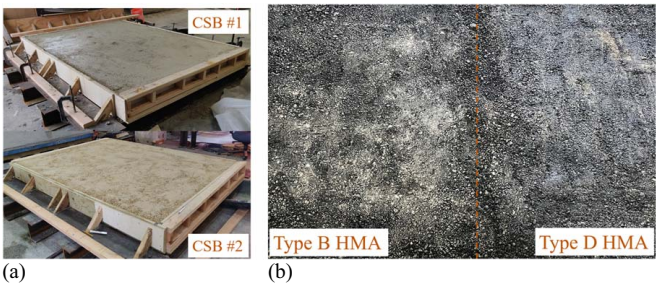

Fig. 11. Phase II bases: (a) CSB specimens; and (b) thin HMA layers.

normal stress levels, which were reached by stacking the slabs, as seen in Fig. 10(a). The concrete slab was quasi-statically loaded with cyclic movements. The loading protocol consisted of eight cycles of fully reversed horizontal displacements at an amplitude of 25 mm (1 in.) representing expansion–contraction cycles.

The cement content by weight of the CSB was 7%. The CSB compressive strengths obtained at 7 days for Specimens #1 and #2 were 5.45 MPa (790 psi) and 6.89 MPa (1,000 psi), respectively. The concrete mix utilized was identical with that used in Phase I.

Phase II: Experimental Results and Discussion

Cyclic Shear Stress–Displacement Relations

Fig. 12 shows selected cyclic shear stress–displacement relationships in Phase II. For the CSB with a double-sided textured LLDPE sheet, the peak was observed in the initial cycle with a normal stress, $\sigma = 8$ kPa (1.17 psi), as shown in Fig. 12(a). This peak can be likely attributed to the effects of interlock. Peaks were also observed in subsequent cycles, but with smaller magnitudes, which was likely attributed to the decrease of the interlocking effects as surface asperities were eroded and initial profiles became more dissimilar. The shear stress–displacement relationship plateaued following movement beyond the initial location. The shear stresses gradually decreased for a few cycles and no significant changes were observed in subsequent cycles. The cyclic behavior observed with either the smooth PE sheets (one and two sheets used) or single-sided spike HDPE sheet was similar to that observed with the textured LLDPE sheet presented in Fig. 12(a).

For the CSB with felt paper, as shown in Fig. 12(b), a significant peak was observed in the initial cycle. The initial peak is attributable to a certain amount of initial bond due to the slight adhesive features of felt paper as well as interlocking effects. Once the initial peak was overcome, the shear stress–displacement curve featured a plateau. In subsequent cycles, there were no obvious peaks because

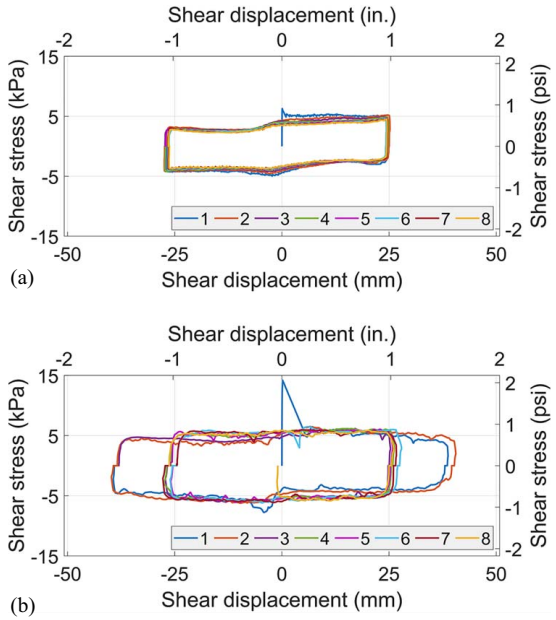

Fig. 12. Phase II cyclic shear stress–displacement relationships ($\sigma =$ 8 kPa/1.17 psi): (a) textured LLDPE sheet (CSB); and (b) felt paper (CSB).

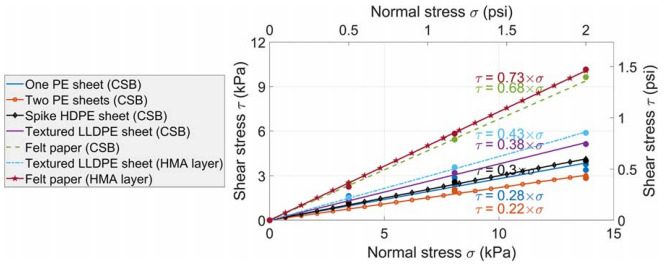

Fig. 13. Phase II steady shear strength envelopes for different bond breakers: Coulomb-friction model.

the concrete block moved beyond its initial placement and the curves were repeatable. The maximum shear displacements were approximately 40 mm (1.5 in.) in each direction for the felt paper specimens.

Interface Shear Strengths and Friction Coefficients

Fig. 13 plots the linearized steady shear strength envelope for the interfaces in Phase II using the Coulomb-friction model. As the figure shows, the linear regression line fits well with the test data, which indicates the absence of adhesion at the slab–base interface. The coefficient of friction in Fig. 13 is given by the slope of the linear regression line. The smooth PE sheets provided the lowest coefficient of friction (from 0.2 to 0.3). The shear strength of one PE sheet was around 25% higher than that of two sheets. With the small surface asperities of the spike HDPE sheet, the coefficient of friction increased slightly to a value of 0.3 compared with the smooth PE sheet. The use of a double-sided textured LLDPE sheet further increased the coefficient of friction to approximately 0.4. Felt paper provided a higher coefficient of friction (approximately 0.7) when compared with the PE sheets. The coefficients of friction obtained with textured LLDPE and felt paper were slightly higher when the CSB surface was topped with a thin Type D HMA layer, as Fig. 13 indicates. This effect can be attributed to the rougher plane of the HMA surface in contact with the interface material when compared with the CSB.

It should be noted that the Phase II series of push-off tests with one and two PE sheets were conducted with two different CSB specimens (Series 1 and 2). This resulted in six sets of data points (σ, τ) per test series, two for each level of normal stress. The six data points obtained for each series are plotted together in Fig. 13 to obtain the shear strength envelopes. The measured shear strength in the case of each normal stress level was consistent between the two specimens. The consistency of the shear stress data indicated that the small variations in the CSB textures did not significantly affect the coefficient of friction at the interface.

Fig. 14(a) compares the steady shear strength envelopes between Series 7a and 7b, in which Type D and Type B HMA were used under the felt paper, respectively. The shear strengths for each normal stress level agree well with each other and the resulting coefficients of friction are relatively close. As shown in Tables 3 and 4, the differences in the aggregate gradation and asphalt content between the thin HMA layer (Type D) and the HMA base (Type B) are not significant. The results indicate that the concrete slab–thin HMA layer interface interaction on top of the CSB is equivalent to that of the concrete slab-HMA base for the same type of bond breaker.

As previously stated, one and two layers of smooth PE sheets on CSB were tested in both Phase I and Phase II. The dimensions of the concrete specimens increased from 0.38 m × 0.38 m × 0.08 m

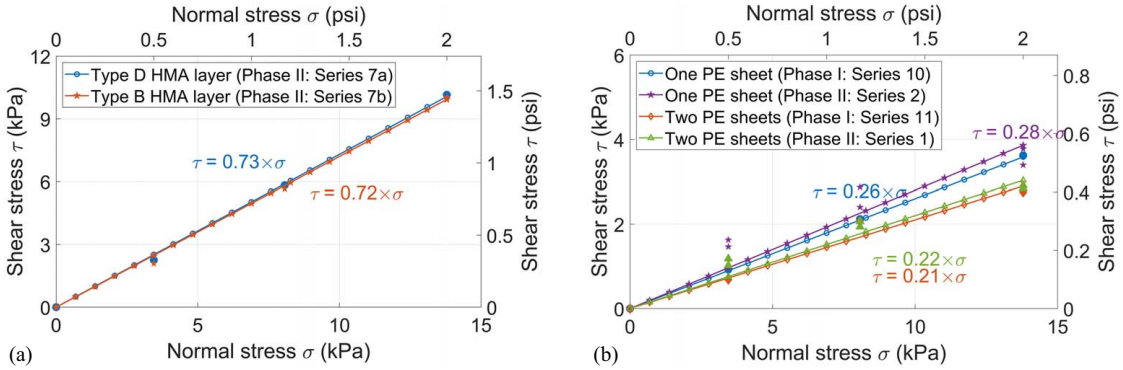

Fig. 14. Comparison results in Coulomb-friction model: (a) Type B and Type D HMA in Phase II; and (b) Phase I and Phase II.

(20 in. × 20 in. × 3 in.) in Phase I to 1.5 m × 0.6 m × 0.15 m (5 ft × 2 ft × 6 in.) in Phase II, which is an increase of more than 620% in the contact surface area. The steady shear strength envelopes are plotted together in Fig. 14(b) for comparison. The steady shear strengths observed in Phase II were approximately 25%–30% higher than those observed in Phase I. These differences can likely be attributed to the finished surfaces of the bases as well as the larger contact surface areas leading to increased interlock. Due to the small-scale specimens used in Phase I, the CSB was compacted via a metal tamper plate driven by a jackhammer, which may have resulted in fewer surface undulations. In Phase II, compaction was carried out with several passes of a plate compactor, which likely produced surfaces that are more consistent with those found in practice. While the Phase I unit-cell direct shear tests were useful in providing a preliminary characterization of interface restraint for different bond breakers, the Phase II full-scale push-off tests should be considered more representative of field conditions and thus provide a more accurate characterization of the slab–base interaction.

Effects of Cyclic Movements

Fig. 15 plots the changes in shear strengths obtained at different cycles of movements for selected interface conditions in Phase II. The values of the peak and steady strength within each cycle are presented in Figs. 15(a and b) for one smooth PE sheet, respectively. The peak strengths obtained for both the forward and the backward sliding movements are plotted for each cycle, as well as the average steady shear strengths in both directions. The peak shear strength in the initial cycle of the first test conducted at a normal stress of 3.5 kPa (0.5 psi) was significantly higher than in subsequent cycles. After five cycles, the peak shear stress stabilized, which can be attributed to a certain smoothing of the profile reducing the effects of interlock. Variation in the steady shear strengths over cycles was

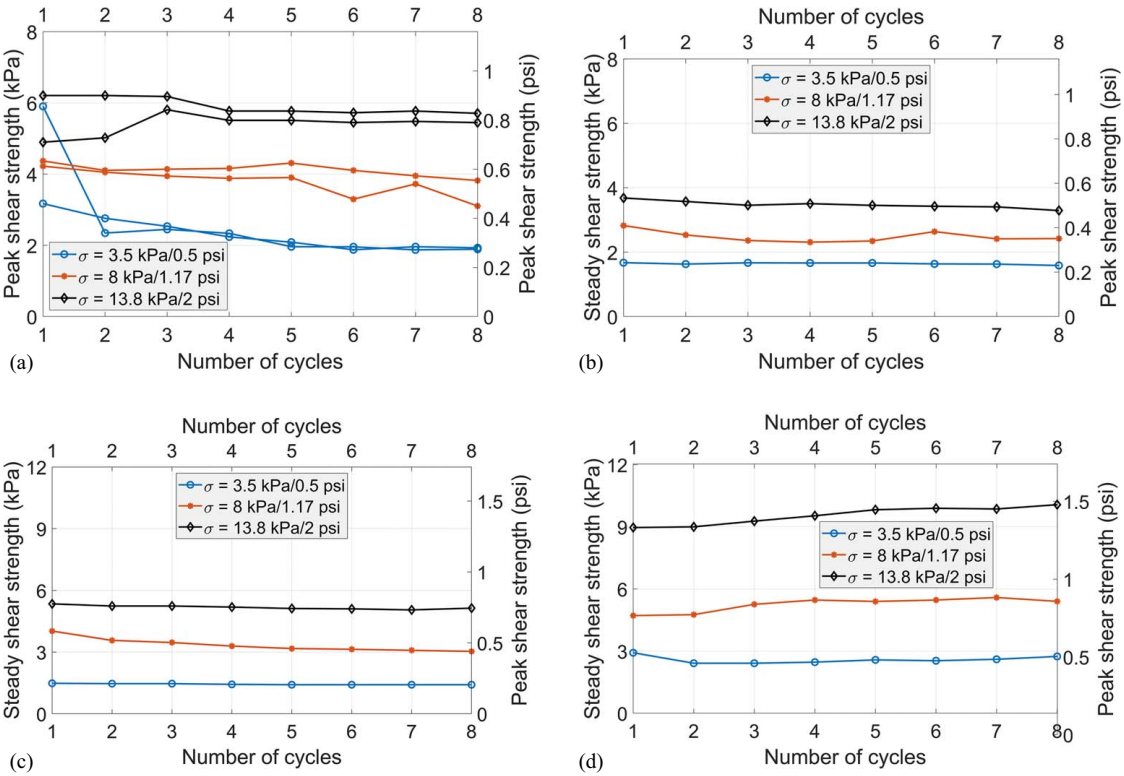

Fig. 15. Effects of the number of cycles on shear strength for different interfaces: (a) peak: one smooth PE sheet (CSB); (b) steady: one smooth PE sheet (CSB); (c) steady: textured LLDPE sheet (CSB); and (d) steady: felt paper (CSB).

Table 8. Phase II failure surfaces

Interface material	Failure surface
Two smooth PE sheets	Between two sheets
One smooth PE sheet	Initially, sheet base; after a few cycles, sheet-CIP concrete.
Single-sided spike HDPE sheet	
Double-sided textured LLDPE sheet	Sheet–base
Felt paper	Felt paper–base

insignificant and similar trends were observed for other bond breakers, as shown in Figs. 15(c and d).

The interface surfaces were visually inspected after the cyclic tests were completed. For the CSB with smooth PE sheets, wrinkles and tearing were observed at several locations of the sheet. The spike HDPE sheet and textured LLDPE sheet presented comparatively less damage, likely due to their relatively larger thickness and density. Felt paper was bonded tightly to the concrete slab with some tearing, while small spalling pieces of felt paper were observed on the base. Overall, the effects of the cyclic movements on the interface restraint were insignificant despite the observed damage to the bond breakers. To reflect significant long-term damage to the bond breaker that may happen over the service life of the seamless bridge, an extreme condition was idealized in which the bond breaker was completely removed. For the specimen with the polyethylene sheet on the CSB, the specimen was lifted and the sheet was removed. The pavement was then tested with concrete on the CSB base. For this specimen, the friction coefficient changed from 0.28 to 0.51. This increase of friction coefficient can be explained by the fact that the interface material not only breaks the bond, but also reduces the frictional restraint between the two concrete surfaces. While the coefficient of friction of approximately 0.50 is representative of the conditions that might occur in the long term, additional studies on the long-term performance are likely prudent.

Sliding Planes

The location of the sliding plane when the steady shear strength was reached was observed in this study. Table 8 summarizes the sliding planes for different interface materials. As shown in the table, sliding in specimens with a double-sided textured LLDPE sheet occurred between the base and the interface material, given that the interface with the CIP concrete achieves some level of bond when concrete is cast against the interface material. Specimens with single PE and HDPE sheets also exhibited an initial slip at the sheet–base interface, but ultimately slid between the sheet and the CIP concrete due to the deterioration of their bond. For two PE sheets, the weakest interface was that between the two sheets.

Table 9. Summary of coefficient of friction for different bond breakers

Base type	Bond breaker	Coefficient of friction (steady)
CSB	Two smooth PE sheets	0.22
	One smooth PE sheet	0.28
	Single-sided spike HDPE sheet	0.3
CSB/CSB with thin HMA/HMA	Double-sided textured LLDPE sheet	0.38–0.43
	Felt paper	0.68–0.73

Design Recommendations for Transition Slab Pavement

Table 9 summarizes the steady coefficients of friction obtained for the different types of bond breakers investigated. The bond breakers are listed in ascending order of their coefficient of friction.

The coefficient of friction of the base–slab concrete interface in the transition zone of a seamless bridge system should be low enough to prevent large tensile stress demands and severe cracking in the concrete slab, but not excessively low to avoid an overly long transition zone. Felt paper and double-sided textured LLDPE sheet are potential bond breakers, which provide a coefficient of friction in the target range of 0.4–0.8, as previously identified based on the Australian experience and preliminary analyses. The felt paper could result in a shorter transition slab due to a relatively large coefficient of friction. From a construction standpoint, both materials are flexible and easy to install, although felt paper is lighter. From a durability standpoint, double-sided textured LLDPE sheets have relatively high tearing resistance and may offer better long-term performance, which was evidenced by the significantly less damage observed in the LLDPE sheets via a visual inspection after the cyclic tests were completed in Phase II.

In summary, the current experimental studies provide adequate estimates of the coefficients of friction for different types of bond breakers and indicate that only minor variations are expected to occur over cyclic movements. Felt paper and double-sided textured LLDPE sheets are identified as two adequate bond breakers for the transition slab in a seamless bridge–CRCP system. However, possible limitations of the laboratory testing in simulating long-term deterioration should be considered when adopting friction coefficients. Parametric numerical studies are still needed to investigate the response of seamless bridge–pavement systems to arrive at general and detailed design recommendations. The construction, instrumentation, and field monitoring of a pilot bridge project with a seamless connection in the United States is recommended for future study, which will provide insights on the long-term field performance of bond breakers.

Conclusions

In this study, concrete pavement–base interaction, which significantly affects the behavior and design of seamless bridge–CRCP systems, was experimentally characterized through a comprehensive testing program. This program consisted of two testing phases in which preliminary unit-cell direct shear tests and full-scale cyclic push-off tests were conducted. The bases investigated included granular bases and stabilized bases (HMA and CSB), which are commonly used in the United States. The testing program explored the effectiveness of different interface materials employed as bond breakers. The interface materials included a 25-mm-thick (1-in.-thick) HMA layer, woven-geotextile, nonwoven geotextile, one or two smooth PE sheets, spike HDPE sheets, textured LLDPE sheets, and felt paper. Shear stress versus displacement up to 25 mm (1 in.) relationships in the case of three normal stress levels of 3.5 kPa (0.5 psi), 8 kPa (1.17 psi), and 13.8 kPa (2 psi), representing the weight of a 0.15-m-/6-in.-, 0.35-m-/14-in.-, and 0.6-m-/24-in.-thick concrete pavement, respectively, were obtained for each type of interface condition. The response of the interfaces was characterized by frictional and adhesion parameters corresponding to Mohr–Coulomb failure criterion. The main conclusions of this study are summarized as follows:

- Concrete–base interfaces with a thin HMA layer, woven geotextile, and nonwoven geotextile presented a strong adhesion and

very high shear strength. As a result, these interface materials are not suitable as bond breakers in transition slabs.

- The use of PE sheets and felt paper eliminated the adhesion at the interface. These interface materials presented σ-τ relations that could be represented well with the classic Coulomb-friction model. The coefficient of friction at large displacements provided by these bond breakers is listed in descending order as follows: felt paper (around 0.7); textured LLDPE sheets (around 0.4); spike HDPE sheets (around 0.3); and smooth PE sheets (around 0.25).
- The concrete specimen–base interfaces with effective bond breakers presented a shear stress–displacement response characterized by a peak shear strength followed by a drop to a large-displacement shear resistance. The peak interface shear strength can be attributed to two sources: (1) an interlocking effect due to the matching profile of the fresh concrete and base generated during casting; and (2) different levels of adhesion of the interface. The magnitude of peak strength was found to decrease after the first cycle of loading due to the decrease of interface interlock, while the shear strength at large displacements was essentially independent of the number of cycles.
- Based on their ability to eliminate adhesion and their adequate range of friction coefficients, felt paper and double-sided textured LLDPE sheets have been identified as adequate bond breakers for the transition slab in seamless bridge–CRCP systems.

Data Availability Statement

Experimental data that support the findings of this study are available from the corresponding author upon reasonable request.

Acknowledgments

This study was sponsored by the Texas Department of Transportation under research project No. 0-7011. Any opinions and findings presented in this paper are those of the authors alone and do not necessarily reflect the opinions of the sponsor. The authors would like to express their gratitude to HDR and Clinton Best for their assistance in obtaining CSB mixtures and technical guidance on CSB construction, and to Martin Marietta Materials, Titan Environmental USA, and Solmax for providing the cement, spike HDPE, and textured LLDPE sheet samples, respectively. The Phase I and Phase II experimental programs were conducted in the Geotechnical Engineering Laboratory and Ferguson Structural Engineering Laboratory at the University of Texas at Austin, respectively. The authors would also like to express their gratitude to the laboratory staff for their technical support.

References

AASHTO. 2020. *LRFD bridge design specifications*. 9th ed. Washington, DC: AASHTO.

Ala, N. 2011. "Seamless bridge and roadway system for the US practice." Ph.D. thesis, Dept. of Civil Engineering, Univ. of Nebraska-Lincoln.

Ala, N., and A. Azizinamini. 2016a. "Proposed design provisions for a seamless bridge system: Cases of flexible and jointed pavements." *J. Bridge Eng.* 21 (2): 04015045.

Ala, N., and A. Azizinamini. 2016b. "Experimental study of seamless bridge transition system for US practice." *J. Bridge Eng.* 21 (2): 04015046.

ASTM. 2016. *Standard specification for asphalt-saturated organic felt underlayment used in steep slope roofing*. ASTM D4869-16. West Conshohocken, PA: ASTM.

ASTM. 2017a. *Standard test methods for compressive strength of molded soil–cement cylinders*. ASTM D1633-17. West Conshohocken, PA: ASTM.

ASTM. 2017b. *Standard specification for plastic water vapor retarders used in contact with soil or granular fill under concrete slabs*. ASTM E1745-17. West Conshohocken, PA: ASTM.

ASTM. 2019. *Standard test methods for moisture–density (unit weight) relations of soil–cement mixtures*. ASTM D588-19. West Conshohocken, PA: ASTM.

ASTM. 2021. *Standard test method for compressive strength of cylindrical concrete specimens*. ASTM C39-21. West Conshohocken, PA: ASTM.

Au, A., C. Lam, J. Au, and B. Tharmabala. 2013. "Eliminating deck joints using debonded link slabs: Research and field tests in Ontario." *J. Bridge Eng.* 18 (8): 768–778.

Burke Jr, M. P. 2009. *Integral and semi-integral bridges*. Hoboken, NJ: Wiley.

Cackler, T., T. Burnham, and D. Harrington. 2018. *Performance assessment of nonwoven geotextile materials used as the separation layer for unbonded concrete overlays of existing concrete pavements in the US*. Ames, IA: National Concrete Pavement Technology Center, Iowa State Univ.

Caner, A., and P. Zia. 1998. "Behavior and design of link slabs for jointless bridge decks." *PCI J.* 43 (3): 68–80.

Chan Suh, Y., S. Woo Lee, and M. Soo Kang. 2002. "Evaluation of subbase friction for typical Korean concrete pavement." *Transp. Res. Rec.* 1809 (1): 66–73.

Chia, W. S., B. F. McCullough, and N. H. Burns. 1986. *Field evaluation of subbase friction characteristics*. Austin, TX: Texas Dept. of Transportation.

Civjan, S. A., C. H. Bonczar, S. F. Breña, J. T. DeJong, and D. S. Crovo. 2007. "Integral abutment bridge behavior: Parametric analysis of a Massachusetts bridge." *J. Bridge Eng.* 12 (1): 64–71.

Griffiths, S., G. Bowmaker, C. Bryce, and R. Bridge. 2005. "Design and construction of seamless pavement on Westlink M7, Sydney, Australia." In *Proc., 8th Int. Conf. on Concrete Pavements*, 21–38. Silver Spring, MD: International Society for Concrete Pavements.

Ha, S., J. Yeon, M. C. Won, Y. S. Jung, and D. G. Zollinger. 2012. *User's guide for TxCRCP-ME design software: Volume I—user's guide and volume II—Software architecture*. Austin, TX: Texas Dept. of Transportation.

Jeong, J. H., J. Y. Park, J. S. Lim, and S. H. Kim. 2014. "Testing and modelling of friction characteristics between concrete slab and subbase layers." *Road Mater. Pavement Des.* 15 (1): 114–130.

Lee, S. W. 2000. "Characteristics of friction between concrete slab and base." *KSCE J. Civ. Eng.* 4 (4): 265–275.

Li, S., B. Tian, K. Niu, Z. Sun, and W. Zhou. 2013. "Characteristics of base friction for concrete pavement structure in China: Experimental study." *Transp. Res. Rec.* 2367 (1): 107–112.

Maitra, S. R., K. S. Reddy, and L. S. Ramachandra. 2009. "Experimental evaluation of interface friction and study of its influence on concrete pavement response." *J. Transp. Eng.* 135 (8): 563–571.

Mohamed, A. M. M. 2017. "Evaluation of soil–reinforcement composite interaction in geosynthetic-reinforced soil structures." Ph.D. thesis, Dept. of Civil, Architectural and Environmental Engineering, Univ. of Texas at Austin.

Otto Rasmussen, R., and D. K. Rozycki. 2001. "Characterization and modeling of axial slab-support restraint." *Transp. Res. Rec.* 1778 (1): 26–32.

Roesler, J. R., J. E. Hiller, and A. S. Brand. 2016. *Continuously reinforced concrete pavement manual, guidelines for design, construction, maintenance, and rehabilitation*. FHWA-HIF-16-026. Washington, DC: Federal Highway Administration.

Stott, J. P. 1961. "Tests on materials for use in sliding layers under concrete road slabs." *Civ. Eng.* 56 (663): 1297.

Thippeswamy, H. K., H. V. GangaRao, and J. M. Franco. 2002. "Performance evaluation of jointless bridges." *J. Bridge Eng.* 7 (5): 276–289.

TxDOT (Texas Department of Transportation). 2014. *Standard specifications for construction and maintenance of highways, streets and bridges*. Austin, TX: TxDOT.
TxDOT (Texas Department of Transportation). 2019. *Pavement manual: Rigid pavement design*. Austin, TX: TxDOT.
White, H. 2007. *Integral abutment bridges: Comparison of current practice between European countries and the United States of America*. Albany, NY: New York State Dept. of Transportation.
Wimsatt, A. J., B. F. McCullough, and N. H. Burns. 1987. *Methods of analyzing and factors influencing frictional effects of subbases*. Austin, TX: Texas Dept. of Transportation.
Wing, K. M., and M. J. Kowalsky. 2005. "Behavior, analysis, and design of an instrumented link slab bridge." *J. Bridge Eng.* 10 (3): 331–344.
Zhan, X., K. Liu, Y. B. Zhao, and H. Yan. 2021. "Tensile performance of SHCC road–bridge link slabs in fully jointless bridges." *Adv. Civ. Eng.* 2021: 1–14.